Development of a module for creep deformation analysis of RPV lower head using shell theory

Jang Min Park[a], Kukhee Lim[b*], Yoonhee Lee[b]
[a]*School of Mechanical Engineering, Yeungnam University, Daehak-ro 280, Gyeongsan, 38541, Republic of Korea*
[b]*Korea Institute of Nuclear Safety, Daejeon, 34142, Republic of Korea*
[*]*E-mail: limkh@kins.re.kr*

***Keywords :** severe accident, RPV lower head failure, shell theory, finite element method

1. Introduction

Under severe accident conditions of nuclear power plants, the reactor pressure vessel may be exposed to high-pressure and high-temperature conditions, increasing the risk of the creep failure in the lower head [1,2]. To evaluate the lower head failure, the severe accident codes, such as MELCOR and MAAP, utilize the membrane model where one-dimensional force balance is considered to predict the effective stress. While this approach is efficient in terms of the computational cost, it falls short in accurately representing the stress state. However, by employing the shell theory [3], stress can be more accurately predicted, resulting in a precise assessment of the lower head failure [1]. The shell theory module had been successfully integrated into the ASTEC code. However, it should be noted that the comprehensive investigation of the performance or characteristics of the shell theory module remains pending.

This study aims to develop an efficient computational model that can represent the creep deformation of the lower head using the shell theory, with particular emphasis on robust mathematical analysis and validation procedures. The existing shell theory is employed [1,2,3], while a minor adjustment has been incorporated to address inherent singularity issues. To account for the large deformation of the lower head due to creep, kinematic equations have been derived. The computational result of the developed module is compared with the finite element analysis result, thereby validating the shell theory module.

Using the developed module, this study also aims to elucidate the extent to which the shell model can accurately capture creep behavior and identify the specific aspects where the model may encounter limitations.

2. Shell Theory

According to the shell theory [1,2,3], the normal forces (N_1 and N_2) and the shear force (Q) acting on a pressurized lower head can be written as follows:

$$N_1 = \frac{p}{r_1}\left(r_2 - \frac{e}{2}\right)\left(r_1 - \frac{e}{2}\right) - \frac{r_2}{r_1}\left(N_2 + \frac{\partial Q}{\partial \psi}\right) - \frac{Q}{r_1}\left(\frac{\partial r_2}{\partial \psi} + r_2 \cot\psi\right), \quad (1)$$

$$N_2 = \frac{p}{2r_2}\left(r_2 - \frac{e}{2}\right)^2 - Q\cot\psi, \quad (2)$$

$$Q(\theta_0) = \frac{pr_a(1-\nu)}{2\lambda}\frac{\exp(-\lambda\theta_0)\cos(\lambda\theta_0)}{\sqrt{\cos(\theta_0 - \alpha\theta_0^2)}}, \quad (3)$$

where p is the applied pressure, e is the thickness, ν is the Poisson ratio, $\lambda = \left(3(1-\nu^2)\left(\frac{r_a}{e_0}\right)^2\right)^{1/4}$, and r_a is the average radius. The force components and kinematic variables are defined in Fig. 1. It should be mentioned that the shear force of Eq. (3) assumes the vessel is hemispherical where the top is fixed [3].

In this study, the shear force is modified because Eq. (3) involves inherent singularity issue at $\theta_0 = \frac{\pi}{2}$ that, in turn, results in the divergence of the normal forces of Eqs. (1) and (2) as $\theta_0 \to \frac{\pi}{2}$. The shifted shear force (Q_s) is written as follows:

$$Q_s(\theta_0) = Q(\theta_0) - Q\left(\frac{\pi}{2}\right). \quad (4)$$

3. Kinematics

The creep deformation results in a significant displacement of the lower head. Therefore, the kinematic variables ψ, r_1, and r_2 in Eqs. (1) to (3) need to be explicitly defined in terms of the coordinates r and θ. By considering an infinitesimal element of the lower head, we could arrive at the relationship for the incline angle ψ as follows:

$$\tan\psi = \frac{r\cos\theta + \frac{dr}{d\theta}\sin\theta}{r\sin\theta - \frac{dr}{d\theta}\cos\theta}. \quad (5)$$

Similarly, the first radius of curvature r_1 can be also derived from the differential calculus as follows:

$$r_1 = -\left(\frac{d\psi}{d\theta}\right)^{-1}\sqrt{r^2 + \left(\frac{dr}{d\theta}\right)^2}. \quad (6)$$

The second radius of curvature r_2 is simply given as follows:

$$r_2 = \frac{x}{\sin\psi} = \frac{r\cos\theta}{\sin\psi}. \quad (7)$$

Meanwhile, the displacement in the $\psi-$ and r_1-directions during the infinitesimal time interval dt are denoted as v and w, respectively, as shown in Fig. 2. They are related to the strain components as follows [3]:

$$\frac{dv}{d\psi} - v\cot\psi = r_1 d\varepsilon_2 - r_2 d\varepsilon_1, \quad (8)$$

$$w = r_2 d\varepsilon_1 - v\cot\psi, \quad (9)$$

where $d\varepsilon_i = \dot{\varepsilon}_i dt$ is the strain increment during the time interval dt. The displacement in the θ- and r-directions are denoted as v' and w', respectively, which are related

to the above displacement components as follows (see Fig. 2):

$$v' = -\sqrt{v^2 + w^2}\cos\alpha, \quad (10)$$

$$w' = \sqrt{v^2 + w^2}\sin\alpha, \quad (11)$$

where the angle $\alpha = \pi - (\theta + \psi) - \arctan\left(\frac{v}{w}\right)$.

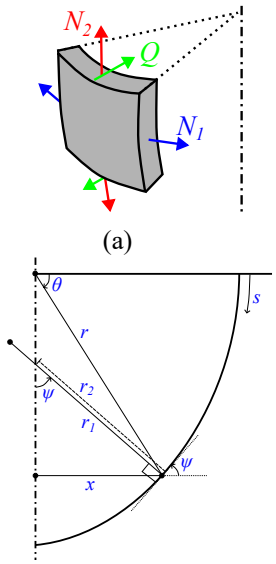

Fig. 1 (a) Force components acting on a shell element and (b) kinematic variables of the lower head.

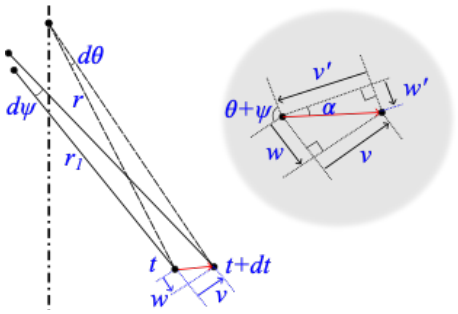

Fig. 2 Displacement during the infinitesimal time interval dt.

4. Constitutive Model

The Norton law is employed to describe the creep deformation as follows [4]:

$$\dot{\varepsilon_c} = \frac{3}{2}\dot{q}\frac{\sigma'}{\sigma_{eq}}, \quad (12)$$

$$\dot{q} = C\sigma_{eq}^m, \quad (13)$$

where C and m are the creep parameters.

5. Finite Element Analysis

Finite element analysis is also carried out for the validation of the developed shell theory module. The Code-Aster, an open-source finite element analysis software is used [6]. The geometrical model is two-dimensional axisymmetric, and quadratic quadrilateral elements are used to discretize the domain. The mesh system comprises 400 elements along the meridian direction and 19 elements along the radial direction.

With regard to the boundary conditions, the displacement is fixed at the top, and pressure is applied to the inner wall, in accordance with the shell theory module.

6. Test Condition

This study considers only the isothermal creep condition for the characterization of the developed shell theory module. Similar to the LHF test condition [5], the average radius ($r_a = \frac{r_i + r_o}{2}$, r_i and r_o are inner and outer radii of the lower head, respectively) is fixed to 0.465 m, and the effective stress ($\sigma_e = \frac{pr_i^2}{r_o^2 - r_i^2}$) is 72.58 MPa. Particularly, the wall thickness of the lower head is varied in this study to examine the performance of the shell theory. Table 1 summarizes the thickness and the applied pressure of the test condition.

The creep parameters C and m are selected as 1×10^{-36} $s^{-1}\text{Pa}^{-m}$ and 4, respectively, so that the creep behavior is similar to that of SA544B1 steel at 1040 K [5].

The failure criterion depends on the failure mode and the material characteristics. In the present shell theory module, the strain is defined as an average value along the thickness. Therefore, the failure criteria based on the average equivalent strain, $\bar{\varepsilon}_{eq} = 0.2$, will be considered. Meanwhile, in the finite element analysis, we apply the strain criterion, $\varepsilon_{eq} = 0.2$, where ε_{eq} is the local equivalent strain [7]. Therefore, the failure in the shell theory module can take place at a larger deformation than in the finite element analysis.

Table 1. Thickness of the lower head and the applied pressure.

Case	Thickness (mm)	Pressure (MPa)
1	30	10
2	50	17.43
3	70	25.55
4	90	34.44

6. Result and Discussion

Fig. 3 compares the shell theory module and the finite element analysis in terms of the maximum value of the equivalent strain. In general, the shell theory module predicts lower strain than the finite element analysis. This is because, in shell theory, we consider the average strain, which should always be lower than the local maxima along the thickness. As the wall thickness is increased, one can find the rate of strain increasing. This reflects that the deformation becomes more localized as the wall thickness is increased.

Fig. 4 shows the initial and final shapes of the lower head for Case 1. The two results agree well in general, while only a minor gap is observed near the top. This gap is because the hoop strain is allowed at the top in the shell

theory module as the radial pressure is assumed constant. Though, this does not affect the global deformation of the lower head, as shown in the figure.

Fig. 5 compares the thickness distribution for Case 1. The shell theory module predicts slightly thinner wall than the finite element analysis does, especially as $\theta \rightarrow \frac{\pi}{2}$. This is because the shell theory module applies the average equivalent strain for the failure criterion, as mentioned before. Though, the gap between the two results is not significant.

Figs. 6 and 7 shows the distribution of the average strain for Case 1. Once again, one can find a general agreement between the shell theory module and the finite element analysis. As mentioned earlier, the shell theory predicts a minor hoop strain ($\bar{\varepsilon}_1$) at the top (Fig. 6). In the finite element analysis result, one can find sharp changes of the meridian ($\bar{\varepsilon}_2$) and radial ($\bar{\varepsilon}_3$) strains, which could not be captured by the shell theory.

As the wall thickness is increased, the disparity between the shell theory and the finite element analysis results becomes more pronounced. For example, Figs. 8 and 9 show the average strain for Case 4, where one can find a larger gap especially as $\theta \rightarrow \frac{\pi}{2}$. The result suggest that the shell theory can be further improved by considering the stress distribution along the thickness direction.

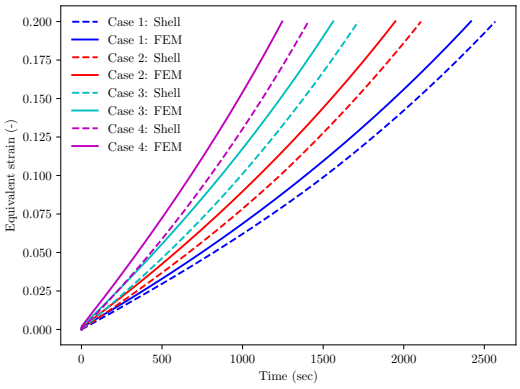

Fig. 3 Maximum equivalent strain versus time.

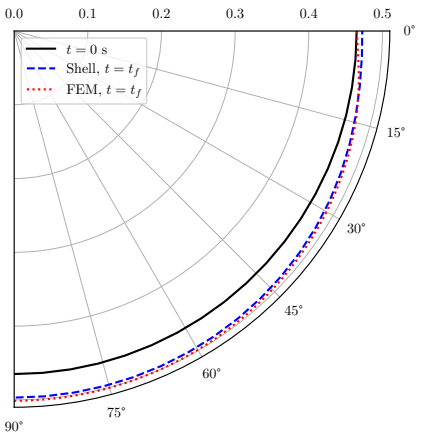

Fig. 4 Initial and deformed shapes for Case 1.

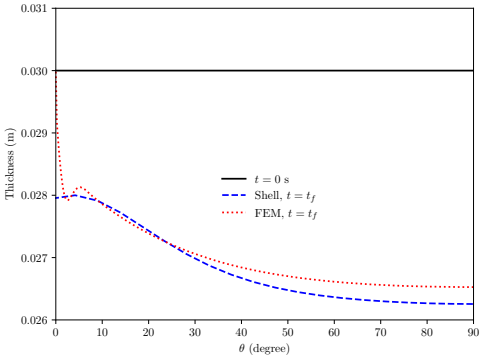

Fig. 5 Thickness of the lower head for Case 1.

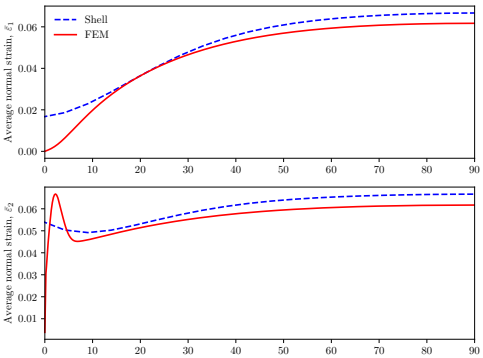

Fig. 6 The average strain $\bar{\varepsilon}_1$ and $\bar{\varepsilon}_2$ for Case 1.

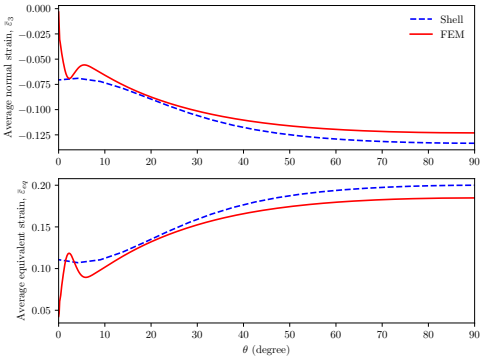

Fig. 7 The average strain $\bar{\varepsilon}_3$ and the average equivalent strain $\bar{\varepsilon}_{eq}$ for Case 1.

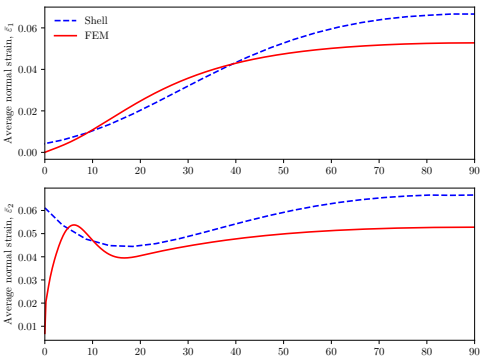

Fig. 8 The average strain $\bar{\varepsilon}_1$ and $\bar{\varepsilon}_2$ for Case 4.

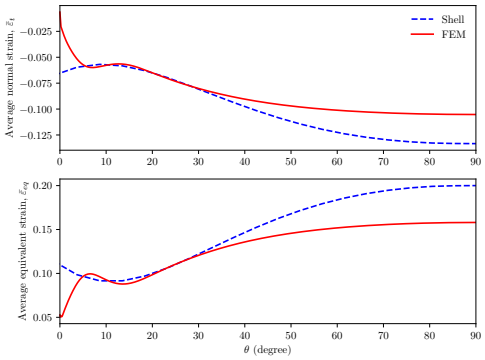

Fig. 9 The average strain $\bar{\varepsilon}_3$ and the average equivalent strain $\bar{\varepsilon}_{eq}$ for Case 4.

7. Conclusions

Built upon the shell theory, this work has developed a computational module capable of describing the creep deformation of the lower head, with particular consideration given to the kinematics of large deformation. The effectiveness of the developed module was assessed by comparing it with the finite element analysis result, demonstrating the validity of the shell theory module.

As the wall thickness is increased, deviations between the shell theory predictions and the finite element analysis results become more noticeable. This result suggests that the shell model could be enhanced by taking into account the stress distribution along the wall thickness, which deserves future study.

Although not presented in this paper, it is also noted the shear force model of Eq. (3) may not be accurate enough, especially for larger deformations where the lower head shape cannot be approximated as a sphere. In this regard, developing an analytical expression of the shear force for ellipsoidal shape also deserves further study in the future.

The creep module developed in this study is expected to be applied to non-isothermal cases that include thermal loads. For this purpose, the creep parameter will be implemented as a function of temperature, which will depend on the position and time.

Finally, it is worth mentioning that the computational time for the shell theory module takes only a few minutes, whereas the finite element analysis demands several hours.

ACKNOWLEDGEMENT

This work was supported by the Nuclear Safety Research Program through the Korea Foundation Of Nuclear Safety (KoFONS) using the financial resource granted by the Nuclear Safety and Security Commission (NSSC) of the Republic of Korea. (No. 2106007).

REFERENCES

[1] V. Koundy and N. H. Hoang, Modelling of PWR lower head failure under severe accident loading using improved shells of revolution theory. Nuclear Engineering and Design, Vol. 238, No. 9, pp. 2400-2410. 2008.
[2] H. Yang, B. Zhang, P. Gao, R. Zhai, and J. Shan, Development and Validation of Thermal-Mechanical Creep Failure Module for Reactor Pressure Vessel Lower Head. Nuclear Science and Engineering, Vo. 197, No. 7, pp. 1436-1453, 2023.
[3] S. Timoshenko and S. Woinowsky-Kreiger, Theory of plates and shells (2nd ed.). McGraw-Hill, pp. 533-554, 1987.
[4] J. Lemaître and J.-L. Chaboche, Mechanics of solid materials. Cambridge University Press, pp. 253-345, 1990.
[5] T.Y. Chu, M.M. Pilch, J.H. Bentz, J.S. Ludwigsen, W.-Y. Lu, L.L. Humphries, Lower Head Failure Experiments and Analyses, Sandia National Laboratories Article NUREG/CR-5582, 1999.
[6] Code_Aster, https://www.code-aster.org/, Accessed 2022.
[7] L. Nicolas, M. Durin, V. Koundy, E. Mathet, A. Bucalossi, P. Eisert, J. Sievers, L. Humphries, J. Smith, V. Pistora, and K. Ikonen, Results of benchmark calculations based on OLHF-1 test. Nuclear Engineering and Design, Vol. 223, No. 3, pp. 263-277, 2003